

DETC2012-71089

## DESIGN AND FABRICATION OF A THREE-DOF MEMS STAGE BASED ON NESTED STRUCTURES

Yong-Sik Kim<sup>1,\*</sup>

<sup>1</sup>Intelligent Systems Division, National Institute of Standards and Technology,  
100 Bureau Drive, Gaithersburg, MD, 20899-8230

Nicholas G. Dagalakis<sup>1</sup>

<sup>1</sup>Intelligent Systems Division, National Institute of Standards and Technology,  
100 Bureau Drive, Gaithersburg, MD, 20899-8230

Satyandra K. Gupta<sup>2</sup>

<sup>2</sup>Mechanical Engineering Department  
University of Maryland at College Park  
College Park, Maryland 20742

### ABSTRACT

*This paper presents the design, fabrication and testing of a Micro Electro Mechanical Systems (MEMS) based positioning stage which is capable of generating translational motions along X, Y and Z axes, respectively. For this purpose, two existing 1 Degree of Freedom (DOF) in-plane positioning stages and one existing 1 DOF out-of-plane actuator are merged into one system for 3 DOF motions. The 1 DOF stage has a platform to embed other systems. For a successful combination of three independent systems, two nested structures are adapted as a serial kinematic mechanism. With nested structures, one 1 DOF in-plane positioning stage is embedded into the other 1 DOF in-plane stage for in-plane translational motions along the X and Y axes. And then, one 1 DOF out-of-plane actuator is embedded for the translational motion along the Z axis. The proposed 3 DOF system has demonstrated ability to generate at least 20  $\mu\text{m}$  along X, Y and Z axes, respectively. The cross talk between the three axes is also measured and is less than 4 percent of the intended displacement.*

*Index terms – MEMS, out-of-plane, electrothermal actuator, eccentric loading  
(Some figures in this article are in color only in the electronic version)*

### INTRODUCTION

Micro Electro Mechanical Systems (MEMS) based positioning stages are attractive at various applications due to the fact that

they can provide not only small footprints and low cost but also nanometer resolution and tens of micro-meters range of motion.

Several existing MEMS based positioning stages have focused on in-plane translational or rotational motions and its combination for 3 or more DOF motion [1 - 5]. This kind of approach comes from MEMS fabrication techniques are limited to planar design and requires considerable efforts for out of plane or the Z axis motion. An XYZ MEMS stage designed for optical scanning and alignment utilizes the collaboration of multiple in-plane actuators with hinge mechanism for out-of-plane motion [2]. Instead of hinges, inclined leaf springs are employed to convert in-plane motion into out-of-plane motion [3]. In these cases, the mechanisms converting to the Z axis motion from in-plane motions are complex to fabricate and friction in the converting mechanisms reduce its lifetime and causes poor performance.

Free of collaboration with in-plane actuators, dedicated out-of-plane actuators for Z axis motion have been developed and adapted for XYZ motion by utilizing a Focused Ion Beam (FIB) milling operation [4] or wafer bonding [5]. With the dedicated Z actuator, the electrostatic actuator generates 1.1  $\mu\text{m}$  displacements at 240 V driving voltage which is similar with its in-plane X or Y axes motion [4] or a 3.5  $\mu\text{m}$  out-of-plane displacement at 14.8 V driving voltages and 25  $\mu\text{m}$  in-plane displacement [5]. Those existing XYZ MEMS stages have their own limitations; (a) due to the electrostatic actuator, its driving voltages are relatively bigger than CMOS-compatible range and (b) its Z displacement is a few micrometer ranges or relatively smaller than its X or Y directional displacement.

With dedicated Z actuators, the relationship between three independent actuators should be established via appropriate kinematic mechanisms. One of commonly used kinematic mechanisms is parallel kinematic mechanism (PKM) [6]. In the PKM, an end-effector has links to all actuators. One of popular links is parallel chains to avoid any rotational errors. With a PKM, the range of motion decreases to the intersection of all the actuators involved and the coupled motion are still left. In addition, a fabrication of parallel chains for Z axis is still challenging at existing MEMS approaches. Another mechanism commonly used in conventional manufacturing is a serial kinematic mechanism (SKM) [7]. In a SKM, each component in the system is connected to only two neighboring components. Each actuator is designated for each axis and combination of three actuators with the serial kinematic mechanism is able to generate 3 DOF motions. Each actuator does not have any mechanical links with the others, so it is expected to have no coupled motion between them and no obstacles to reduce its range of motion.

Various MEMS actuators have been adapted for positioning stages [1, 5, 7]. Commonly used actuators are electrostatic [1, 5] or electrothermal actuator [7, 8]. The electrostatic actuator has wider bandwidth and better energy efficiency than the electrothermal actuator, but the

electrothermal actuator has a smaller footprint, CMOS-compatible driving voltage and mill-newton level force generation [8].

This paper presents the design and fabrication of an XYZ MEMS positioning stage which is capable of generating translational motions along X, Y and Z axes. For more than tens of  $\mu\text{m}$  range along the X, Y, and Z axes, electrothermal actuators and a serial kinematic mechanism are selected. Two existing in-plane 1 DOF motion stages and one existing out-of-plane motion stage are utilized for XYZ motion. The demonstration with fabricated devices shows tens of  $\mu\text{m}$  range of motion without acceptable coupled errors.

## DESIGN AND ANALYSIS

The proposed XYZ MEMS stage consists of two in-plane stages and one out-of-plane actuator. Two equivalent in-plane 1 DOF stages are selected from previous research due to the fact that it has a platform to utilize for a SKM [7, 9]. Figures 1(a) and 1(b) show a Computer Aided Design (CAD) schematic diagram of the chosen single DOF stage. The stage in Figure 1(a) (called the X stage) and Figure 1(b) (called the Y stage) are aligned with the X and Y axes respectively and the Y stage is embedded into the platform in the X stage for in-plane X and Y translational motions. An out-of-plane electrothermal actuator,

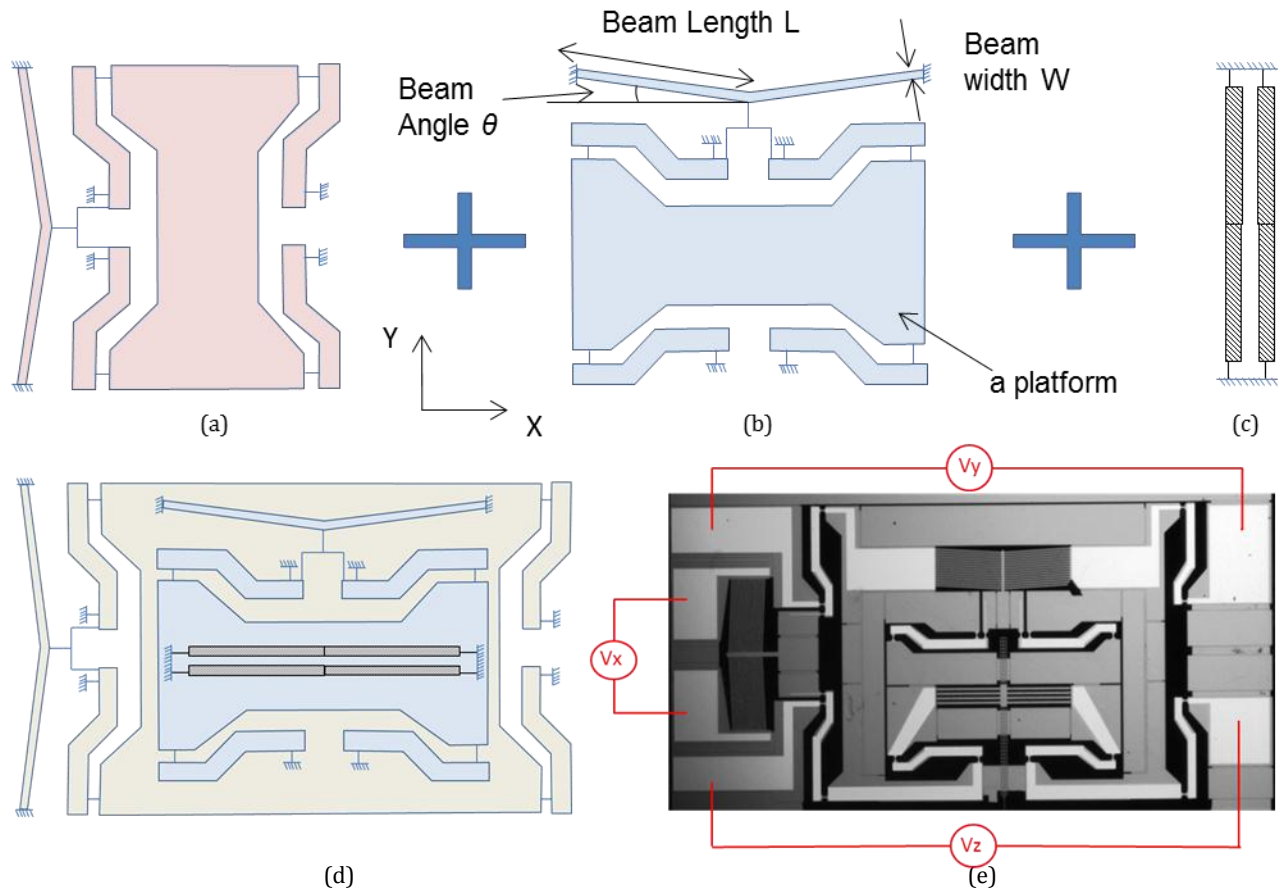


**Figure 1.** a schematic diagram of the XYZ MEMS stage and its fabrication; (a) X stage; (b) Y stage; (c) Z axis actuator; (d) combination of the three independent systems for XYZ stage; (e) a fabricated device based on (d)

shown in Figure 1(c) (called a Z actuator) is embedded in the platform in the Y stage for a translational motion along the Z axis. Details about the Z actuator are in [10]. The main reasons to select this actuator are; (a) it can be fabricated based on the standard Silicon on Insulator-Multi User Multi Process (SOI-MUMPs) [11] without significant modification and (b) this actuator can generate at least 20  $\mu\text{m}$  displacement. These three separate components are mechanically merged together via two nested structures as a SKM and the final design is shown in Figure 1(d). The fabricated device is shown in Figure 1(e), where the driving voltage  $V_x$  is connected to the two pads for the X stage,  $V_y$  for the Y stage and  $V_z$  for the Z actuator. The connections for  $V_y$  and  $V_z$  utilize links and flexures surrounding the platform in the X stage and the Y stage, respectively. The chip size is 4 mm x 7 mm

### 1. Design of the in-plane stage

The adapted X and the Y stages consist of an electrothermal actuator, four links and a platform and shown in Figure 1(b). For low acceleration these stages can be approximated as two springs in a series. With this serial connection, the expected displacement of the moving platform can be expressed as:

$$U_{\text{platform}} = \frac{F_{\text{actuator}}}{K_{\text{actuator}} + K_{\text{platform}}} \quad (1)$$

Where,  $U_{\text{target}}$ ,  $K_{\text{target}}$  are the displacement and the stiffness of the platform, respectively.  $F_{\text{actuator}}$  is a force generated by the actuator to move the platform and can be expressed based on beam theory as:

$$F_{\text{actuator}} = 2\alpha\Delta T_{\text{ave}}EWT\sin\theta \quad (2)$$

Where,  $\alpha$  is the coefficient of thermal expansion of silicon,  $\Delta T_{\text{ave}}$  is the average temperature over the actuator,  $E$  is the Young's modulus of silicon and  $W$ ,  $T$ ,  $L$  and  $\theta$  are beam width, thickness, length and angle, respectively. The average temperature generated by Joule heating in the actuator can be found [12] and expressed as:

$$\Delta T_{\text{ave}} = \frac{V^2}{3k\rho} \quad (3)$$

The stiffness of the electrothermal actuator can be expressed [13] as:

$$K_{\text{act}} = 2\left(\sin^2\theta + \cos^2\theta \frac{12I}{WTL^2}\right) \frac{EWT}{L} \quad (4)$$

where  $I$  is the area moment of inertia. The stiffness of the stage can be expressed as:

$$K_{\text{stg}} = \frac{n^2m}{L_1^2C_z} \quad (5)$$

Where,  $n$  is the lever ratio,  $m$  is the number of the flexure hinges used in the target platform and  $L_1$  is a link length.  $C_z$  is its angular compliance about Z axis of the flexure hinge and derived by the Paros and Weisbro formula [14].

$$U_{\text{target}} = \frac{2\alpha EWT\sin\theta}{6k\rho\left(\sin^2\theta + \cos^2\theta \frac{12I}{WTL^2}\right) \frac{EA}{L} + \frac{R^2m}{L_1^2C_z}} V^2 \quad (6)$$

Based on equation (6), the expected displacement of the target platform can be expressed by a square of the driving voltage. Based on all equations described above, all the design parameters are determined and listed in table 1 below.

### 2. Design of the out-of-plane actuator

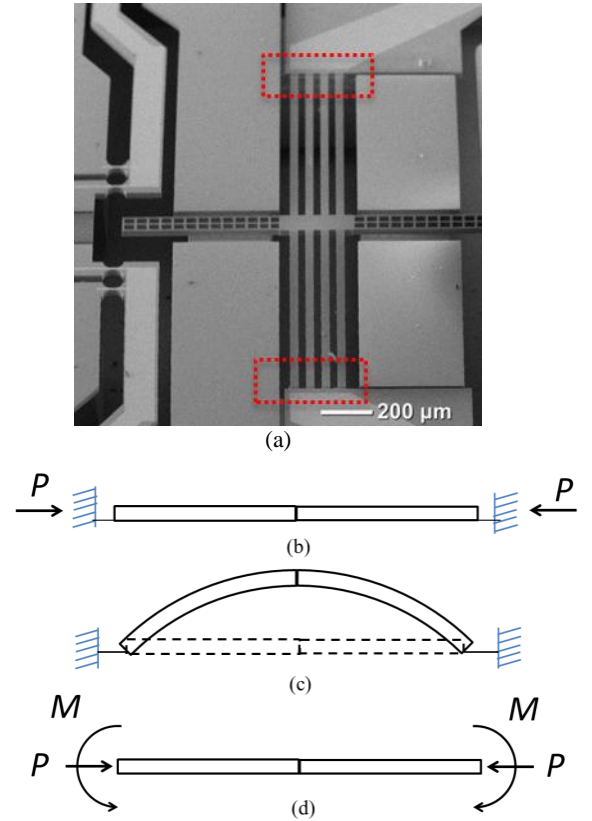


**Figure 2.** the Z actuator; (a) fabricated out-of-plane actuator; (b) a schematic diagram of the actuator; (c) an expected mechanical behavior during operation; (d) converted free-body diagram based on (b)

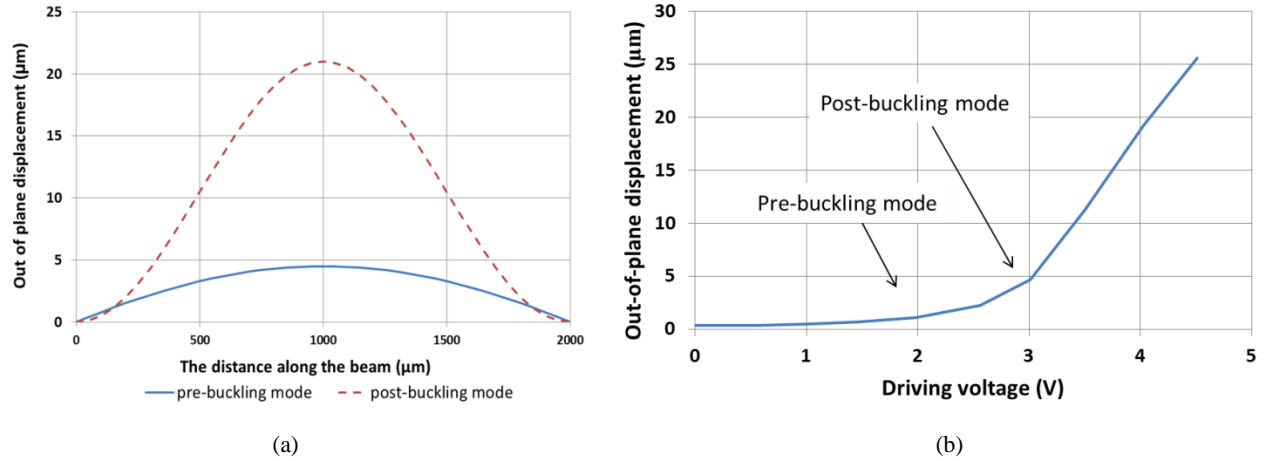


**Figure 3.** the Z actuator; (a) an expected deformation profile of the out-of-plane actuator at pre- and post-buckling mode; (b) experimental results

The Z actuator is composed of a pair of notches and beams and shown in Figure 2(a), where the Z actuator is embedded into the proposed system. The notches at both ends are indicated by red boxes in Figure 2(a) and the schematic diagram of the Z actuator is shown in Figure 2(b). The beams with notches convert Joule heating into an eccentric load. This eccentric load deforms the beam convex shape at the pre-buckling mode and shown in Figure 2(c). After a pre-buckling mode, the actuator keeps generating out-of-plane motion at post-buckling mode.

The eccentric load  $P$  can be converted into one centric load and a moment as shown in Figure 2(d). With this converted free-body diagram, the expected deformation profile at pre-buckling mode can be expressed [15] based on its fixed-fixed boundary conditions.

$$y = e \left[ \tan \left( L \sqrt{\frac{P}{EI}} \right) \sin \left( \sqrt{\frac{P}{EI}} x \right) + \cos \left( \sqrt{\frac{P}{EI}} x \right) - 1 \right] \quad (7)$$

for driving voltage  $\leq 3$  V

where,  $P$  is the eccentric load and  $e$  is the distance from the central line of the beam to middle of the notch. With higher driving voltage (more than 3 V in the proposed actuator), the beam begin to buckle and post-buckling becomes dominant. By assuming fixed-fixed boundary conditions, the deformation profile can be expressed [16] as:

$$y = H \left( 1 - \cos \frac{2n\pi}{L} x \right) \quad \text{for driving voltage} > 3 \text{ V} \quad (8)$$

where,  $H$  is the amplitude of the post-buckling mode, which is indeterminate. This is due to the fact that equation (8) comes from a linearized approximation of the real governing equation of the beam elastic curve. With measured value  $H$  from the experiments, the expected deformation profiles at pre- and post-buckling mode beam displacement are plotted in Figure 3(a). The relationship between the out-of-plane displacement and the driving voltage is obtained from

experiments and shown in Figure 3(b). Buckling starts at 3 V with current design and its out-of-plane displacement accelerates at post-buckling mode.

Based on equations (6), (7) and (8), the design parameters for each component are selected and listed in table 1.

Symbol	Design parameters	Values
W	Beam width of the in-plane actuator	22.3 $\mu\text{m}$
n	Number of the in-plane actuator	15
$\theta$	Beam angle of the in-plane actuator	3.99 $^\circ$
T	Beam thickness of the in-plane actuator	30 $\mu\text{m}$
L	Beam length of the in-plane actuator	1000 $\mu\text{m}$
p	Notch depth of the out-of-plane actuator	15 $\mu\text{m}$
$W_1$	Beam width of the out-of-plane actuator	33 $\mu\text{m}$
$L_1$	The length of the link connected to the platform	1000 $\mu\text{m}$
m	Number of flexure hinges utilized in the platform	8
R	The lever ratio of the platform	10/1

**Table 1.** The list of the design parameters

## MICRO-FABRICATION

The proposed MEMS XYZ stage is fabricated on both sides of a silicon-on-insulator (SOI) wafer using mainly Deep Reactive Ion Etching (DRIE). The fabrication process follows SOI-MUMPs [11] and consists of two etchings on the top side, one etching on the bottom side and metal depositions for electric pads and lines. The SOI wafer used in the fabrication consists of a 30  $\mu\text{m}$  thick device layer (top side), a 400  $\mu\text{m}$  thick handle layer (bottom side), and a 2  $\mu\text{m}$  thick buried oxide layer. Details are shown in Figure 4.

Figure 5 shows some fabricated features related to electric issues. Figure 5(a) shows the electric connection to the Y stage or the Z actuator over the flexure hinge. With this connection, all electric connections to the Y stage and the Z actuator can be controlled outside the X stage. In addition, to avoid any electric coupled motion between stages and the actuator, each actuator is electrically isolated from platforms with physical gaps and

shown in Figure 5(b). The top side has gaps, which are held their shape by additional features beneath them. This additional feature such as block is made of the bottom side silicon. A built-in probe is attached to the Z actuator for future applications and shown in Figure 5(c).

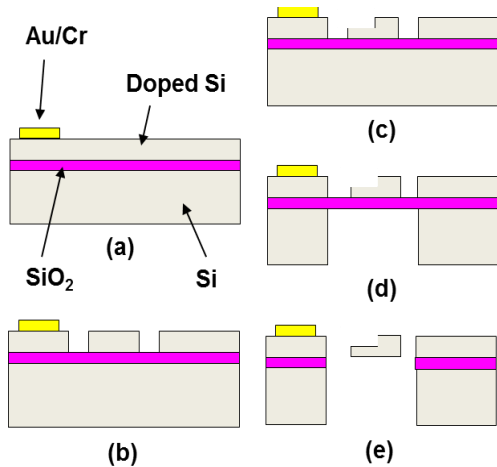


**Figure 4.** Fabrication sequence: (a) metal deposition for electrical connection; (b) first etching for the main structures on the top side; (c) second etching for the Z actuator on the top side; (d) third etching on the bottom side to open the bottom side of the devices; (e) the removal of the buried oxide layer with B.H.F. to release the stage

## EXPERIMENTAL RESULTS

### 1. The range of motion and its coupled motion

The range of motion and its coupled motion are experimentally measured with fabricated XYZ stage samples. The measured ranges along the X, the Y and the Z axes are plotted in Figure 6. The displacement of the X and Y stages and the Z actuator are measured at 23.9  $\mu\text{m}$ , 25.3  $\mu\text{m}$  and 21.2  $\mu\text{m}$  respectively for driving voltages 8 V, 7 V and 6 V, respectively. With less than 10 V, each DOF is able to generate at least 20  $\mu\text{m}$  displacements from this experiment. The relationship

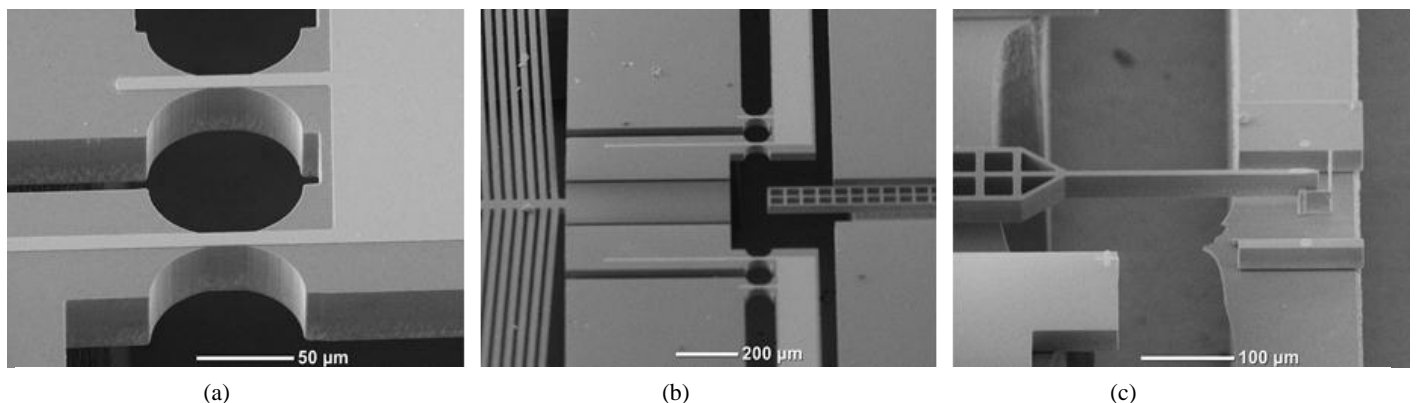
between a driving voltage and its displacement shows the pattern described in equation (6); the displacement is proportional to the square of the driving voltage. In-plane X stage is identical with the in-plane Y stage except the platform size, but the mechanical behavior of the Y stage is slightly different from the X stage. This comes from the difference at thermal boundary condition. The Y stage is connected via four links to the X stage which is directly linked to the fixed ground. In this case, the Y stage tends to keep higher temperature than the X stage with a same driving voltage. The minimum step size in the in-plane motion depends on the electric devices and sensors employed for this system. With optical microscope, 1  $\mu\text{m}$  step was repeated. But the previous experiments on this design demonstrated that 50 nm step size was possible [9].

Table 2 summarizes the coupled motion or unwanted motions along X, Y or Z axes during operation. When one stage or actuator is in operation, the coupled motions along the other two axes are measured at the same time. The coupled motions occurred at the Z actuator by the actuation of the X and the Y stages are relatively smaller than the others, because the Z actuator does not have any platforms and then is stiffer than the others. But, the Z actuator causes 4.1 % coupled motion to the X stage, because the beams in the Z actuator are parallel with the X axis.

The test results show that the proposed system is capable of generating at least 20  $\mu\text{m}$  displacement along the X, Y and Z axes with less than 4.1 percent coupled motions.

### 2. The frequency response

Frequency response of the proposed XYZ stage is measured experimentally along X, Y and Z axes, respectively. For in-plane X-and Y-axes, Agilent<sup>1</sup> Fast-Fourier-Transform (FFT) dynamic analyzer is utilized. The response is measured with an intensity-based laser reflectometer. More details on the experimental set-ups are given in [17]. Figures 7(a) and 7(b) show the frequency response results along X and Y axes. The first oscillatory mode resonance of the X stage occurs at 680 Hz and the corresponding mode resonance of the Y stage occurs at



**Figure 5.** (a) an electric connection over a flexure hinge; (b) an electric isolation between an actuator and a platform; (c) a built-in probe for future application during operation

<sup>1</sup> Certain commercial equipment is identified in this paper to adequately describe the experimental procedure. Such identification does not imply recommendation or endorsement by the National Institute of Standards and Technology nor does it imply that the equipment identified is necessarily the best available for the purpose.

Actuation		Coupled motion					
		X		Y		Z	
axis	displacement s	displacements	ratio	displacement s	ratio	displacement s	ratio
X	23.9 $\mu\text{m}$	-	-	0.8904 $\mu\text{m}$	3.7 %	0.007 $\mu\text{m}$	0.02 %
Y	25.3 $\mu\text{m}$	0.4593 $\mu\text{m}$	1.8 %	-	-	0.0161 $\mu\text{m}$	0.06 %
Z	21.2 $\mu\text{m}$	0.9185 $\mu\text{m}$	4.1 %	0.4595 $\mu\text{m}$	2.0 %	-	-

**Table 2.** Experimental displacement and cross talk error results between X, Y and Z axes

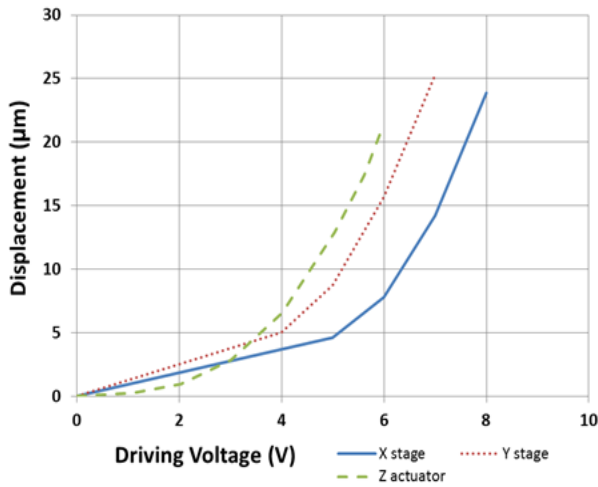


**Figure 6.** a range of motion along X, Y and Z axes versus driving voltage

approximately 1.05 kHz. Since the X stage supports the Y stage and the Z actuator, it is more massive and thus has a lower resonant frequency than that of the Y stage, although they are almost identical in design.

The frequency response along the Z axis is measured by a Polytec<sup>1</sup> MSA-500 Micro System Analyzer [18]. By integrating a microscope and a scanning laser Doppler vibrometer, this analyzer measures the frequency response for out-of-plane motion. Figure 7(c) shows its frequency response along Z axis. The first oscillatory mode resonance of the Z axis is near 78.3 kHz, which is similar with its FEA result. The frequency is

much higher than the other two because the Z stage does not have any platforms.

## CONCLUSION AND DISCUSSION

This paper describes an XYZ MEMS nanositioning stage capable of producing translational motions along X, Y and Z axes. The proposed system is implemented by nested structures and based on a serial kinematic mechanism. For this purpose, two 1 DOF in-plane stages are adapted as the X and the Y stages and an out-of-plane actuator is selected as the Z actuator. With two nested structures, all three independent systems are merged into a single system for XYZ motion. The merged system forms a serial kinematic mechanism, so the Z stage is embedded into the Y stage. The Y stage is then embedded into the X stage. This system is fabricated based on standard SOI MUMPs [11].

The nanopositioner demonstrated 23.9  $\mu\text{m}$  x 25.3  $\mu\text{m}$  x 21.2  $\mu\text{m}$  range displacements along X, Y and Z axes with 8 V, 7 V, 6 V driving voltages, respectively. These are not their maximum allowable range of motion. After careful study on fatigue, failure or plastic deformation, the maximum allowable range of motion needs to be measured again. During operation, the coupled motions were also measured and found to be less than 4.1 % of the associated motion. Special features for electric isolation and backside holding structure should be carefully evaluated to reduce its coupled motion. The frequency response along X, Y, and Z axes was also measured and found to have oscillatory mode resonances at 680 Hz, 1.05 kHz and 78.3 kHz, respectively.

The in-plane 1 DOF stage utilized in the proposed system

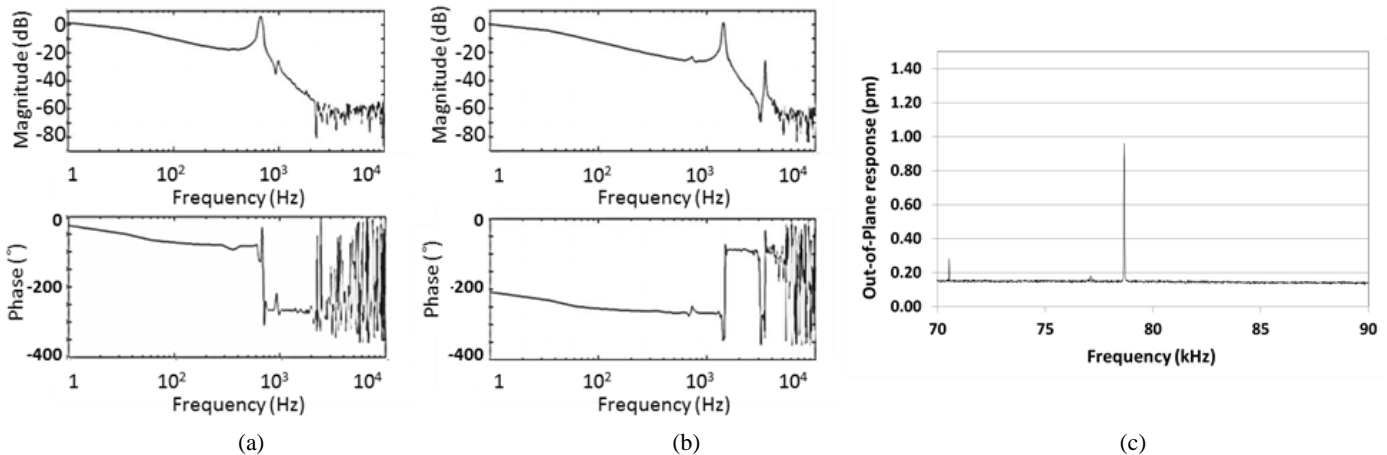


**Figure 7.** Frequency response graphs for; (a) the X stage; (b) the Y stage; (c) the Z stage

is over-constrained for in-plane motion, so any unwanted motion for in-plane motion can be eliminated by this structure. But there are no such a mechanisms in the Z actuator, so guiding mechanism or constraining mechanism for Z axis motion is needed.

The dual nested structures for a SKM can be utilized for further applications such as micro-grippers or embedded active feedback sensors by replacing the Z actuator with grippers or piezoresistive sensors.

## ACKNOWLEDGMENTS

The authors would like to thank Dr. Richard Gates and Dr. Seung Ho Yang for their valuable support on the frequency response measurement. This research was supported by the NIST Next Generation Robotics and Automation program and was performed in part in the NIST Center for Nanoscale Science and Technology Nano Fabrication Clean Room.

## REFERENCES

[1] D. Mukhopadhyay, J. Dong, E. Pengwang, P. Ferreira, "A SOI-MEMS-based 3-DOF planar parallel-kinematics nanopositioning stage," *Sensors and Actuators A* 147 (2008) 340-351

[2] Fan L, Wu M C, Choquette K D and Crawford M H 1997 Self-assembled microactuated XYZ stage for optical scanning and alignment Proc. Int. Conf. Solid-State Sensors and Actuators (Chicago, IL) pp 319–22

[3] Takahashi K, Mita M, Fujita H and Toshiyoshi H 2007 Topological layer switch technique for monolithically integrated electrostatic XYZ-stage Proc. IEEE MEMS (Kobe, Japan) pp 651–4

[4] Ando Y 2004 Development of three-dimensional electrostatic stages for scanning probe microscope *Sensors Actuators A* 114 285–91

[5] X. Liu, K. Kim, Y. Sun, "A MEMS stage for 3-axis nanopositioning," *J. Micromech. Microeng.* 17 (2007) 1796-1802

[6] Q. Yao, J. Dong, P. M. Ferreira, Design, analysis, fabrication and testing of a parallel-kinematic micropositioning XY stage, *International Journal of Machine Tools and Manufacture*, Vol. 47, Issue 6, May 2006, pp 85-95

[7] Kim YS, Nicholas NG, Gupta SK 2011 A Two Degree of Freedom Nanopositioner with Electrothermal Actuator for Decoupled Motion, ASME/IDETC conference, DC, USA

[8] L. Que, JS Park, YB Gianchandani, 2001 "Bent-beam electrothermal actuators-Part I: Single beam and cascaded devices," *J. of MEMS*, Vol. 10(2), pp 247 – 254

[9] Bergna S, Gorman J J, Dagalakis N G 2005 Design and Modeling of Thermally actuated MEMS Nanpositioner Proc. of IMECE2005, 2005 ASME International Mechanical Engineering Congress and Exposition, Orlando, Florida USA

[10] Kim YS, Nicholas NG, Gupta SK 2012 Design, fabrication and characterization of a single-layer out-of-plane electrothermal actuator for SOI-MEMS applications, PerMIS'12 March 20-22, College Park MD USA

[11] Miller K, Cowen A, Hames G and Hardy B SOIMUMPs Design Handbook revision 4.0", in <http://www.memscap.com/mumps/documents/SOIMUMPs.dr.v4.pdf>

[12] Luo J L, Flewitt A J, Spearing S M, Fleck N A and Milne W L 2005 Three types of planar structure microspring electro-thermal actuators with insulating beam constraints *J. Micromech. Microeng.* 15 pp 1527-1535

[13] Zhu Y, Corigliano A and Espinosa H D 2006 A thermal actuator for nanoscale in situ microscopy testing: design and characterization *J. Micromech. Microeng.* 16 242-253

[14] J. M. Paros and L. Weisbord, "How to design flexure hinges," *Machine Design* 37 (27) 1965 pp151-156

[15] F. P. Beer, E. R. Johnston, JR. "Mechanics of Materials," 2nd edition McGraw-Hill, 1992, pp 650-652

[16] Johnes R M 2008 Buckling of Bars, Plates, and Shells pp 73-75

[17] Gorman J J, Kim Y S and Dagalakis N G 2006 Control of MEMS Nanopositioners With Nano-Scale Resolution ASME Proc. of the ASME International Mechanical Engineering Conference and Exhibition Chicago USA

[18] Polytec MSA-500 Micro System Analyzer, in "<http://www.polytec.com/us/products/vibration-sensors/microscope-based-systems/>"